J Mater Sci (2011) 46:3337–3342
DOI 10.1007/s10853-010-5221-x

Mn_3O_4/worm-like mesoporous carbon synthesized via a microwave method for supercapacitors

Tianxiang Zhou · Shanshan Mo · Shuangli Zhou · Wujun Zou · Yingliang Liu · Dingsheng Yuan

Received: 19 September 2010 / Accepted: 24 December 2010 / Published online: 8 January 2011

Abstract A quick and facile microwave method has been employed to prepare Mn_3O_4/worm-like mesoporous carbon (Mn_3O_4–MC) composites. Structural and morphological characterizations of worm-like mesoporous carbon and Mn_3O_4–MC composites have been carried out using X-ray diffraction, transmission electron microscopy, N_2 adsorption–desorption, and electrochemical measurement. Cyclic voltammograms demonstrate that the Mn_3O_4–MC composites perform improved capacitive behavior at the range of $-0.8 \sim 0.2$ V (vs. Hg/HgO electrode) with reversibility. The Mn_3O_4–MC composite electrode possesses an enhanced specific capacitance of 266 F g^{-1} at a sweep rate of 1 mV s^{-1}.

Introduction

Supercapacitors are novel charge-storage devices of high power density, which exhibit excellent reversibility and a long cycle life [1–4]. Supercapacitors can be categorized electrical double-layer capacitor (EDLC) and Faradic pseudocapacitor on the basis of the charge-storage mechanism. EDLC based on carbon electrodes stores energy by charge accumulation at the electrode/electrolyte interface. With regard to Faradic pseudocapacitor, it is owing to the reversible Faradic redox reactions at the surface of electrodes, which have been prepared with metal oxides and conducting polymers. Therefore, it is clearly that the electrode materials are the key in the development of supercapacitors. Nowadays, mesoporous carbon and carbon-based composite electrode materials have been mostly investigated and commercially applied to supercapacitors.

Mesoporous carbons can be used as host materials to synthesize composite systems with special properties. On the other hand, some transition metal oxides based on pseudocapacitance for charge-store [5, 6], such as NiO [7], Co_3O_4 [8], IrO_2 [9], RuO_2 [10–12], have been investigated as the potential electrode materials in neutral aqueous electrolytes for supercapacitors; Manganese oxides have received tremendous attention for pseudocapacitors not only due to their low cost but also to their environmental-friendly characteristics [13]. Manganese oxides contain MnO, MnO_2, Mn_2O_3, and Mn_3O_4 due to the existence of Mn in different oxidation states (+2, +3, and +4). Among them, Mn_3O_4 is seen to be a promising and low cost catalyst for various reactions such as the oxidation of carbon monoxide, methane [14] and the reduction of nitrobenzene [15]. It is also an air pollution control material for reducing industrial and environmental emission [16]. Various synthetic methods have been employed for preparing Mn_3O_4, such as thermal decomposition [17], coprecipitation method [18], hydrothermal method [19], and so on.

Up to now, considerable effort has been made to focus on the fabrication of carbon-based nanocomposite materials, because it has an important effect on the development of electronic applications, advanced catalysts, and adsorption [20]. Therefore, various metal oxide nanoparticles had been deposited on carbon materials, For example, MnO_2/carbon [21–24], Bi_2O_3/carbon [25], and Mn_3O_4/carbon [26]. These composites had been used as electrode materials for electrochemical supercapacitors and as an air diffusion electrode material to be studied the electrocatalytic performance for the oxygen reduction. However, to the best of our knowledge, no literature has been reported

T. Zhou · S. Mo · S. Zhou · W. Zou · Y. Liu · D. Yuan (✉)
Department of Chemistry, Institute of Nanochemistry, Jinan University, Guangzhou 510632, China
e-mail: tydsh@jnu.edu.cn

on Mn_3O_4/mesoporous carbon composite as supercapacitance materials.

Herein, we report the preparation of Mn_3O_4/worm-like mesoporous carbon (Mn_3O_4–MC) composites via a quick and facile microwave method using an aqueous solution of $Mn(NO_3)_2$ as the precursor of the oxidant of Mn_2O_3 and mesoporous carbon as the reductant. The X-ray diffraction (XRD) and the transmission electron microscopy (TEM) indicate that Mn_3O_4 is successfully loaded on worm-like mesoporous carbon. The as-prepared Mn_3O_4–MC composites present high electrochemical performance.

Experimental part

Sample preparation

Worm-like mesoporous carbon (WMC) was prepared via metal–organic coordination polymers (MOCPs) as a template and glycerol as carbon precursor according to our previous reported procedure [27]. The obtained WMC was immersed into 0.1, 0.5, and 1 mol L^{-1} $Mn(NO_3)_2$ and stirred vigorously for 40 min. The mixture was filtered and dried at 100°C for 1 h, then put into the microwave oven to heat via microwave irradiation with a moderate power (~400 W) for 60 s. Subsequently, Mn_3O_4–MC composite materials were obtained.

Characterization of Mn_3O_4–MC composite materials

The structure of as-prepared Mn_3O_4–MC was analyzed by a MSAL-XD2 X-ray diffractometer (Cu Kα, 36 kV, 20 mA, $\lambda = 1.54056$ Å). The morphologies were examined on a PHILIPS TECNAI-10 transmission electron microscope using an accelerating voltage of 100 kV. The specific surface areas of Mn_3O_4–MC were performed via the Micromeritics TriStar 3000 analyzer.

Electrochemical performance

The working electrode was fabricated by pressing the mixture of active materials, carbon black and 5%-PTFE (75:15:10 wt%) into foam nickel electrode. All electrochemical measurements were conducted on a CHI 660B electrochemical workstation. The experiments were carried out in a standard three-electrode cell containing a nickel foil electrode as a counter electrode and an Hg/HgO (6.0 mol L^{-1} KOH) as a reference electrode and the above-mentioned electrode as working electrode. Cyclic voltammetry and galvanostatic charge/discharge was employed to measure the performance of the electrode materials in aqueous electrolyte of 6.0 mol L^{-1} KOH.

Results and discussions

The Mn_3O_4–MC are prepared using $Mn(NO_3)_2$ aqueous solution with concentrations of 0.1, 0.5, and 1 mol L^{-1}, denoted as Mn_3O_4–MC-0.1, Mn_3O_4–MC-0.5, and Mn_3O_4–MC-1. Based on the previous studies [1, 28, 29], the synthesis mechanism of Mn_3O_4–MC composites may be described as follows: an aqueous solution of a Mn^{2+} salt is impregnated into the mesoporous carbon, dried and heated in microwave oven converts the precursor to Mn_2O_3, then Mn_2O_3 is reduced to Mn_3O_4 by mesoporous carbon and without destroying the mesostructure. The Mn_3O_4 content of the Mn_3O_4–MC-1 composite is measured to be the highest by ICP analysis, up to 43 wt%, Mn_3O_4–MC-0.5 and Mn_3O_4–MC-0.1 are 29 and 10 wt%, respectively. The loading amount of Mn_3O_4 depends on the concentration of $Mn(NO_3)_2$, the larger concentration of Mn $(NO_3)_2$ is, the more the loading amount of Mn_3O_4 becomes.

The XRD patterns of Mn_3O_4–MC are given in Fig. 1b–d. These patterns for the Mn_3O_4–MC present diffraction peaks at $2\theta = 18.0°$, 29.0°, 32.4°, 36.1°, 58.5°, 59.9°, and 64.6° corresponding to the (101), (112), (103), (211), (321), (224), and (400) (JCPDS No. 89-4837) planes of Mn_3O_4, respectively, which can be ascribed to the characteristic peaks of the tetragonal cell of Mn_3O_4 structure (Hausmannite). Nevertheless, no peaks attributable to any other oxidation state of manganese are observed, indicating the high purity of the Mn_3O_4 phase in the composites. With the increase of $Mn(NO_3)_2$ solution concentration, the characteristic peaks of the Mn_3O_4 become stronger, which indicates the loading amount of Mn_3O_4 is more. In addition, Fig. 1a also exhibits the XRD pattern of WMC, in which only two broad diffraction peaks at 24.6° and 44.2° are observed, corresponding to the (002) and (101) (JCPDS No. 75-1621) facets of hexagonal graphitic carbon, respectively. A broad peak around 24.6° indicates that the sample synthesized contains amorphous carbon. The average size (D_{hkl}) of Mn_3O_4 particles in the Mn_3O_4–MC-0.5 is estimated to be 32.9 nm on the basis of the Mn_3O_4 (211) peak by Scherrer's equation:

$$D_{hkl} = \frac{0.89\lambda}{B\cos\theta} \quad (1)$$

where λ is X-ray wavelength, B is diffraction peak of full width at half maximum, and θ is diffraction angle.

Figure 2 shows TEM images of WMC and Mn_3O_4–MC-0.5. A lot of Mn_3O_4 nanoparticles are well dispersed on the surface of the mesoporous carbon (Fig. 2b). Increasing $Mn(NO_3)_2$ solution concentration, particle size of Mn_3O_4 has a slight enlargement. The typical size of Mn_3O_4 nanoparticles is about 30 nm, which is in good agreement with the calculated value from XRD patterns.

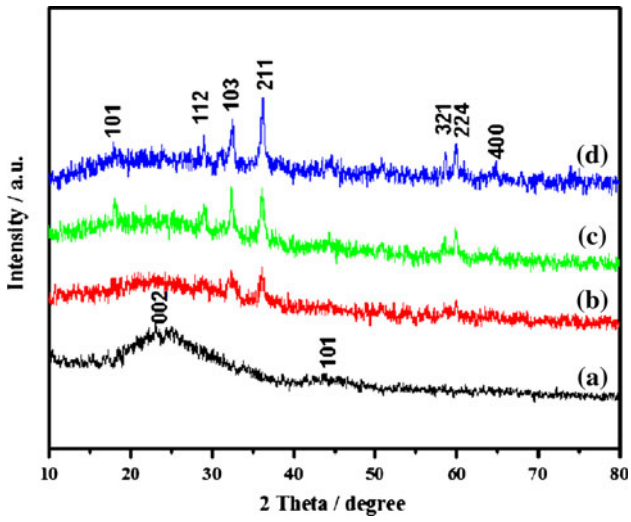

Fig. 1 XRD patterns of (*a*) WMC, (*b*) Mn_3O_4–MC-0.1, (*c*) Mn_3O_4–MC-0.5, and (*d*) Mn_3O_4–MC-1

The pore structure and surface area of WMC, Mn_3O_4–MC-0.1, Mn_3O_4–MC-0.5, and Mn_3O_4–MC-1 are investigated by N_2 adsorption–desorption method, as shown in Fig. 3a. All samples are found to yield a type IIb isotherm with an H_3 hysteresis loop, which is typically associated with non-rigid and disordered mesopores [30]. The experimental results reveal that the mesoporous structure of WMC has been well kept. The BET specific surface areas (Table 1) of WMC, Mn_3O_4–MC-0.1, Mn_3O_4–MC-0.5, and Mn_3O_4–MC-1 are measured to be 1824, 1532, 989, and 638 $m^2\ g^{-1}$, respectively. The surface area gradually decreases with increase of the concentration of $Mn(NO_3)_2$. Similarly, the pore volume also decreases from 2.69 $cm^3\ g^{-1}$ for WMC to 0.87 $cm^3\ g^{-1}$ for Mn_3O_4–MC-1. These mainly result from the higher density of Mn_3O_4 than that of carbon rather than the pore-filling by Mn_3O_4, as being confirmed by the data of average pore size and TEM images. The pore size distributions for WMC and Mn_3O_4–MC composites are shown in Fig. 3b. Their pore size distributions calculated from the adsorption branches by the Barrett–Joyner–Halenda method are centered at 5.9, 5.4, 5.3, and 5.2 nm from WMC to Mn_3O_4–MC-1 (Table 1). The negligible pore size change seen from the pore size distribution curves demonstrates that the Mn_3O_4 nanoparticles do not form in the small mesopores of WMC but to produce on the surface and big mesopores and macropores. The electrochemical behaviors are strongly influenced by the pore size distribution of the carbon materials. The pores larger than 2 nm in diameter are suitable for aqueous electrolyte [31]. It is demonstrated that Mn_3O_4–MC composites could be an excellent electrode material for the electrochemical supercapacitors.

In order to evaluate the electrochemical characteristics of WMC and Mn_3O_4–MC composites, cyclic voltammograms (CVs), galvanostatic charge/discharge and cycle life tests have been carried out to characterize the electrochemical capacitance performance. Figure 4a gives the CVs of WMC and Mn_3O_4–MC composites electrodes in 6.0 mol L^{-1} KOH aqueous solution ranged from −0.8 to 0.2 V with a sweep rate of 5 mV s^{-1}. CVs of WMC are close to a rectangular shape. However, one pair of redox peaks exists in CVs of Mn_3O_4–MC composites, which indicates the visible increase of capacitance for Mn_3O_4–MC composites. We study the time of microwave irradiation and the concentration of $Mn(NO_3)_2$ in detail. An optimum synthesis condition is the time of 60 s and the $Mn(NO_3)_2$ concentration of 0.5 mol L^{-1}. The synthesized Mn_3O_4–MC-0.5 exhibits the largest specific capacitance (Fig. 4a). It is probably related to the suitable porous structure of WMC for electric double-layer capacitance and the appropriate loading of Mn_3O_4 for contributing to the pseudocapacitance. The comparison of galvanostatic charge/discharge curves for the WMC and Mn_3O_4–MC electrodes at a current density of 1 A g^{-1} is shown in Fig. 4b. The variation of potential is linear with time of the charge/discharge for WMC. However, the charge/discharge curves of Mn_3O_4–MC electrodes are asymmetry, which

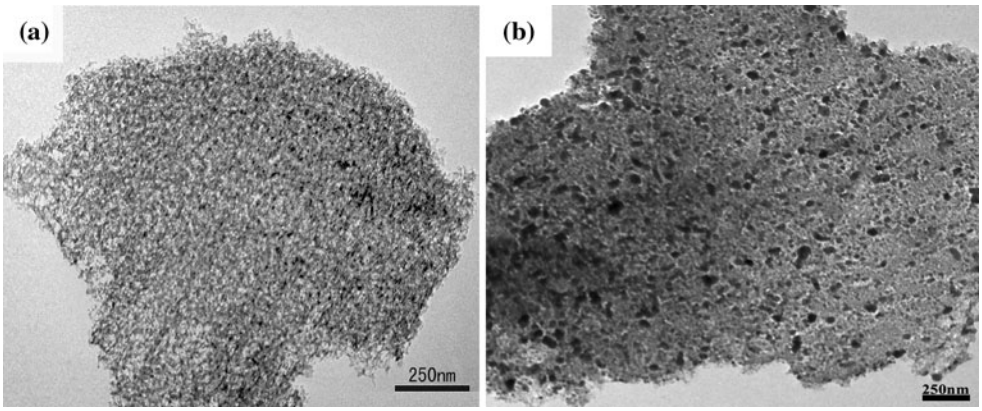

Fig. 2 TEM images of (**a**) WMC and (**b**) Mn_3O_4–MC-0.5

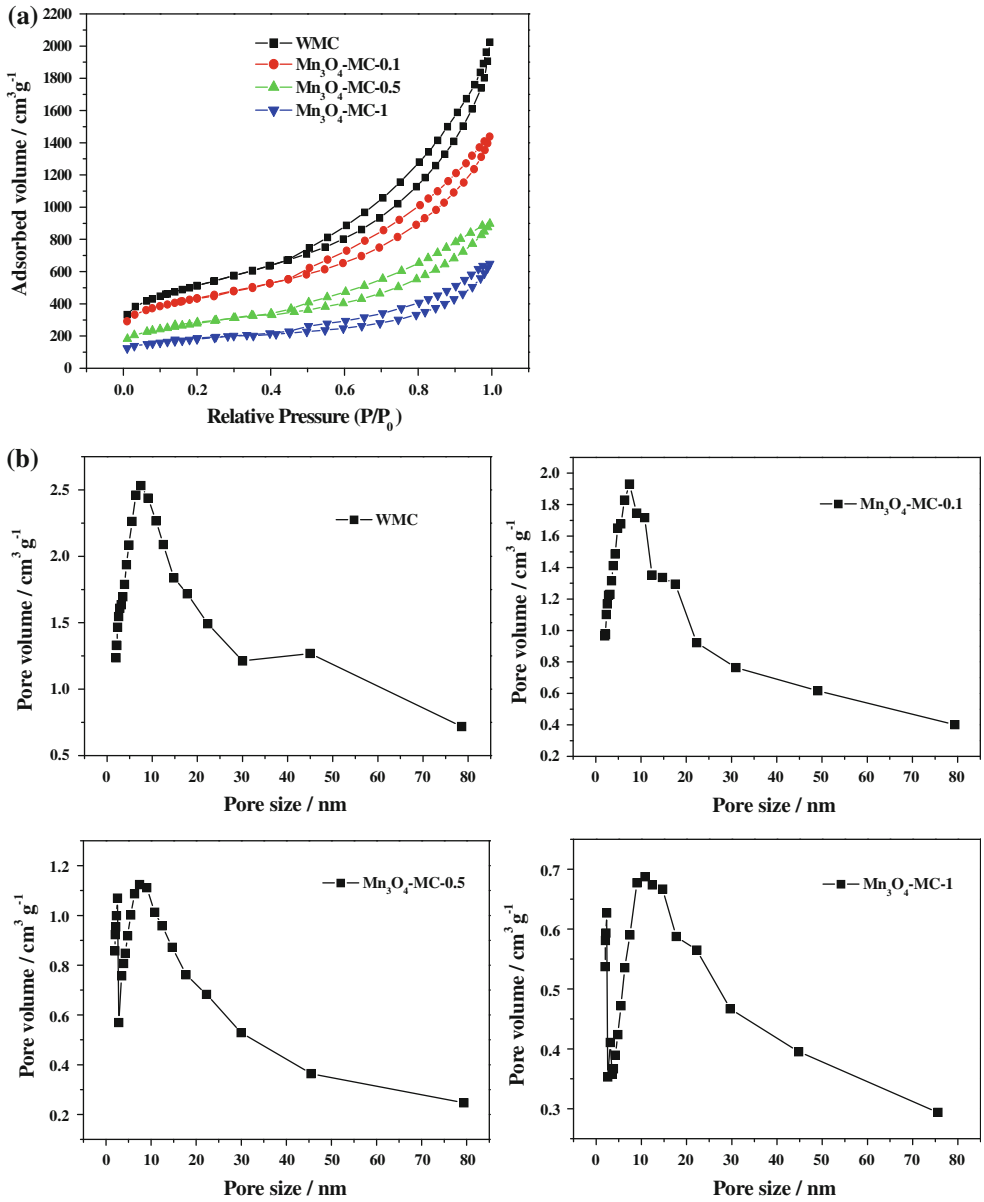

Fig. 3 (**a**) N_2 adsorption–desorption isotherms and (**b**) the pore size distribution of WMC and Mn_3O_4–MC composites

Table 1 Pore structure parameters of the WMC and Mn_3O_4–MC composites and the capacitance of WMC and Mn_3O_4–MC composites electrodes calculated from CVs

Sample	S_{BET} (m^2 g^{-1})	V (cm^3 g^{-1})	D (nm)	Specific capacitance (F g^{-1})					
				1 mV s^{-1}	5 mV s^{-1}	10 mV s^{-1}	20 mV s^{-1}	50 mV s^{-1}	100 mV s^{-1}
WMC	1824	2.69	5.9	162	147	141	133	123	108
S-0.1	1532	2.03	5.4	226	206	200	194	164	139
S-0.5	989	1.28	5.3	266	228	226	205	167	139
S-1	638	0.87	5.2	195	153	147	135	114	95

S_{BET} BET surface area, V pore volume, D pore size, S Mn_3O_4–MC

further verify that Mn_3O_4 contributes the pseudocapacitance. Figure 4c and d presents CVs of WMC and Mn_3O_4–MC-0.5 electrodes under the different sweep rates. The CVs of WMC retain a similar shape at high sweep rates, which indicates the unrestricted motion of electrolytes in the pores of WMC during the double-layer formation and

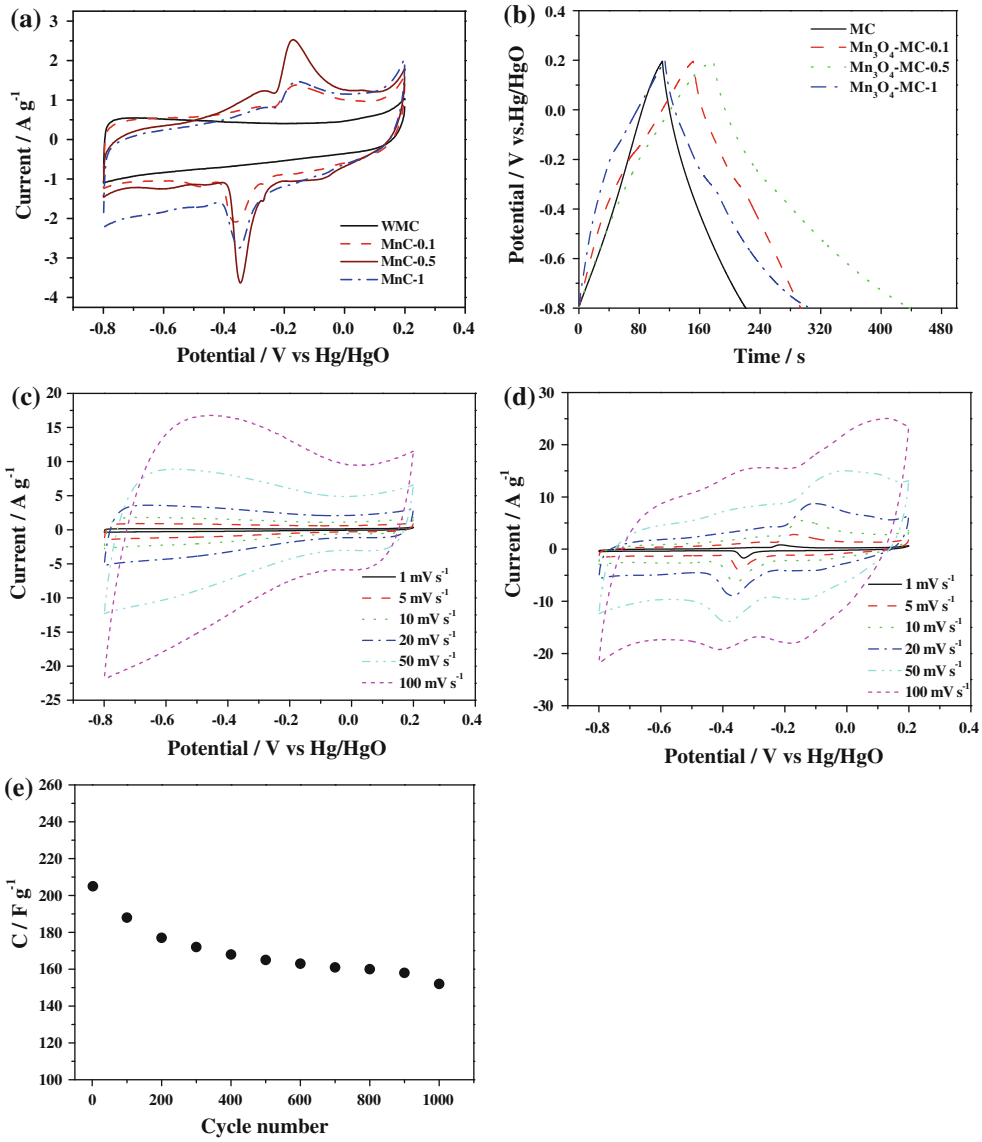

Fig. 4 (**a**) CVs of WMC and Mn_3O_4–MC composites at sweep rate of 5 mV s^{-1}; (**b**) Charge/discharge curves of WMC and Mn_3O_4–MC composites at current density of 1 A g^{-1}; (**c**, **d**) CVs of WMC and Mn_3O_4–MC-0.5 at different sweep rates. (**e**) Cycle life for Mn_3O_4–MC-0.5 measured at sweep rate of 20 mV s^{-1}

also reflects that the ohmic resistance for electrolyte motion in carbon mesopores is small [32]. CVs of Mn_3O_4–MC-0.5 electrode present the redox peaks. And the redox peaks gradually become wider with sweep rate increase, it should also be noted that with the increase of sweep rate, a positive shift of oxidation peaks and a negative shift of reduction peaks are observed, which is mainly due to the resistance of the electrode [33].

The specific capacitance (C) of electrodes is calculated from the CVs according to the following equation [32]:

$$C = \frac{Q}{WV} = \frac{\int i dt}{W \Delta V} \quad (2)$$

where i, W, and ΔV are the sample current, the weight of active materials and the total potential deviation of the voltage window, respectively. The data calculated from CVs of WMC and Mn_3O_4–MC composites is also listed in Table 1. The specific capacitance of Mn_3O_4–MC-0.5 reaches 266 F g^{-1} at the sweep rate of 1 mV s^{-1} and improves 64% compared with WMC (162 F g^{-1}), corresponding to the pseudocapacitive behavior of manganese oxides. The capacitance decreases with the increase of sweep rate. This can be attributed to two reasons. One is due to the ionic diffusion process within micropores to be inhibited at fast sweep rate, causing no response to capacitance. The other reason is: the response of redox reactions intensely depends on the insertion–deinsertion of ions from the electrolyte to Mn_3O_4 at different sweep rate. Thus, at low sweep rate, the ionic diffusion from the electrolyte can gain access to all available pores of the Mn_3O_4, leading to a complete insertion reaction. Therefore, it shows almost ideal capacitive behavior. Whereas the sweep rates are increased, electric charges might have some difficulty to

occupy the available sites at electrode/electrolyte interface due to their limited rate of migration and orientation in the electrolyte [34]. The pseudocapacitance mechanism of manganese oxides in aqueous solution is proposed by Reaction 1:

$$MnO_x(OH)_y + \delta H_2O + \delta e^- \leftrightarrow MnO_{x-\delta}(OH)_{y+\delta} + \delta OH^- \quad (1)$$

where $MnO_x(OH)_y$ and $MnO_{x-\delta}(OH)_{y+\delta}$ indicate interfacial manganese oxide under the higher and lower oxidation states, respectively. Cycle life test for Mn_3O_4–MC-0.5 is measured by cyclic voltammetry at 20 mV s^{-1} for 1000 cycles (see Fig. 4e). The specific capacitance of active materials drops down from 205 to 152 F g^{-1} after 1000 cycles.

Conclusions

In summary, Mn_3O_4/worm-like mesoporous carbon is successfully synthesized via the microwave method. Mn_3O_4 nanoparticles are well dispersed on the surface of WMC, resulting in the decrease of surface area and pore volume due to the increase of weight ratio of Mn_3O_4 in composites. However, Mn_3O_4–MC composites perform the improvement for specific capacitance compared with pure WMC. The specific capacitance of Mn_3O_4–MC-0.5 is as high as 266 F g^{-1} at the sweep rate of 1 mV s^{-1}. The capacitance loss of Mn_3O_4–MC-0.5 is 25.8% after 1000 cycles. The unique performance makes Mn_3O_4–MC composites as the potential candidates for the application in electrode materials of electrochemical capacitors.

Acknowledgements The authors wish to acknowledge financial support from the National Natural Science Foundation of China (20876067 and 21031001) and the Fundamental Research Funds for the Central Universities (21609203).

References

1. Dong XP, Shen WH, Gu JL, Xiong LM (2006) J Phys Chem B 110:6015
2. Li GR, Feng ZP, Ou YN, Wu DC, Fu RW, Tong YX (2010) Langmuir 26:2209
3. Malak-Polaczyk A, Matei-Ghimbeu C, Vix-Guterl C, Frackowiak E (2010) J Solid State Chem 183:969
4. Zhang LL, Wei TX, Wang WJ, Zhao XS (2009) Microporous Mesoporous Mater 123:260
5. Toupin M, Brousse T, Be′ langer D (2004) Chem Mater 16: 3184
6. Toupin M, Brousse T, Be′ langer D (2002) Chem Mater 14:3946
7. Lee JY, Liang K, An KH, Lee YH (2005) Synth Met 150:153
8. Kim HK, Seong TY, Lim JH, Cho WI, Yoon YS (2001) J Power Sources 102:167
9. Hu CC, Huang YH, Chang KH (2002) J Power Sources 108:117
10. Zhao YM, Liu L, Xu J, Yang J, Yan MM, Jiang ZY (2007) J Solid State Electrochem 11:283
11. Jang JH, Han SJ, Hyeon T, Oh SM (2003) J Power Sources 123:79
12. Li HF, Wang RD, Cao R (2008) Microporous Mesoporous Mater 111:32
13. Hu CC, Tsou TW (2003) J Power Sources 115:179
14. Stobbe ER, Boer BA, Geus JW (1999) Catal Today 47:161
15. Yamashita T, Vannice A (1996) J Catal 163:158
16. Vázquez-Olmos A, Redón R, Rodríguez-Gattorno G, Mata-Zamora ME, Morales-Leal F, Fernández-Osorio AL, Saniger JM (2005) J Colloid Interface Sci 291:175
17. Morsali A, Monfared HH, Morsali A (2009) J Mol Struct 938:10
18. Finocchio E, Busca G (2001) Catal Today 70:213
19. Du GH, Van tendeloo G (2008) Appl Phys A 91:393
20. Fan J, Wang T, Yu CZ, Tu B, Jiang ZY, Zhao DY (2004) Adv Mater 16:1432
21. Lei YN, Fournier C (2008) Microporous Mesoporous Mater 110:167
22. Yoon SH, Lee CW, Seung MO, Park YK, Choi WC (2009) J Non-Cryst Solids 355:252
23. Wang XQ, Wilson B et al (2010) J Mater Chem 20:390
24. Mastro MA, Eddy CR, Kub F et al (2009) Surf Rev Lett 16:513
25. Yuan DS, Zeng JH, Kristian N, Wang Y, Wang X (2009) Electrochem Commun 11:313
26. Wang YG, Cheng L, Li F, Xiong HM, Xia YY (2007) Chem Mater 19:2095
27. Yuan DS, Chen JX, Tan SX, Xia NN, Liu YL (2009) Electrochem Commun 11:1191
28. Jiao F, Harrison A, Hill AH, Bruce PG (2007) Adv Mater 19:4063
29. Ramesh K, Chen LW, Chen FX, Zhong ZY, Chin JH, Mook HW, Han YF (2007) Catal Commun 8:1421
30. Sing KSW, Everett DH, Haul RAW, Moscou L, Pierotti RA, Rouqoerol J, Simieniewska T (1985) Pure Appl Chem 57:603
31. Burke A (1995) In: Proceedings of the workshop on carbon for Li-ion battery, supercapacitor. US Department of Energy, Reno, Nevada
32. Yuan DS, Zeng JH, Chen JX, Liu YL (2009) Int J Electrochem Sci 4:562
33. Wang YG, Li HQ, Xia YY (2006) Adv Mater 18:2619
34. Sivaraman P, Rath SK, Hande VR, Thakur AP, Patri M, Samui AB (2006) Synth Met 156:1057